HHS Public Access

Author manuscript

Angew Chem Int Ed Engl. Author manuscript; available in PMC 2021 June 02.

Published in final edited form as:

Angew Chem Int Ed Engl. 2020 June 02; 59(23): 8833–8838. doi:10.1002/anie.201914384.

A simple phototheranostics strategy to continuously deliver singlet oxygen in dark and hypoxic tumor microenvironment

J Zou[1,2], **J Zhu**[1], **Z Yang**[*,2], **L Li**[2], **W Fan**[2], **L He**[2], **W Tang**[2], **L Deng**[2], **J Mu**[2], **Y Ma**[2], **Y Cheng**[2], **W Huang**[1,3], **X Dong**[*,1], **X Chen**[*,2]

[1]Key Laboratory of Flexible Electronics (KLOFE) &, Institute of Advanced Materials (IAM), Nanjing Tech University (NanjingTech), 30 South Puzhu Road, Nanjing, 211800, China

[2]Laboratory of Molecular Imaging and Nanomedicine (LOMIN), National Institute of Biomedical Imaging and Bioengineering (NIBIB), National Institutes of Health (NIH), Bethesda, MD 20892, USA

[3]Shaanxi Institute of Flexible Electronics (SIFE), Northwestern Polytechnical University (NPU), 127 West Youyi Road, Xi'an 710072, China

Abstract

Continuous irradiation during photodynamic therapy (PDT) process inevitably induces tumor hypoxia, thereby weakening the PDT effect. In the PDT induced temporary hypoxia, sustainably providing singlet oxygen from stored chemical energy may enhance the cell killing effect and boost the phototheranostics. Herein, we present a phototheranostics (DPPTPE@PEG-Py NPs) by using 2-pyridone based diblock polymer (PEG-Py) to encapsulate a semiconducting heavy atom free pyrrolopyrrolidone-tetraphenylethylene (DPPTPE) with high singlet oxygen generation ability both in dichloromethane and water. In the phototheranostics, the designed PEG-Py can trap the $^1O_2$ generated from DPPTPE under laser irradiation and form a stable intermediate of endoperoxide, which can then chemically release $^1O_2$ in both dark and hypoxic tumor microenvironment. In comparison with DSPE-PEG encapsulated DPPTPE (DPPTPE@DSPE-PEG), much lower half maximum inhibitory concentration (IC_{50}) was observed in four types of cancer cell lines, including HeLa, HCT-116, A549 and MCF-7 under laser irradiation after being uptaken by DPPTPE@PEG-Py NPs. Furthermore, the fluorescence imaging guided phototherapy study demonstrates that our designed phototheranostics could completely inhibit the tumor growth with the help of laser. This study provides a paradigm to develop highly efficient photosensitizers with photodynamic and photothermal capability for personalized cancer therapy.

Graphical Abstract

* iamxcdong@njtech.edu.cn, zhen.yang3@nih.gov; shawn.chen@nih.gov.

Conflict of interest

The authors declare no conflict of interest.

Supporting information for this article is given *via* a link at the end of the document.

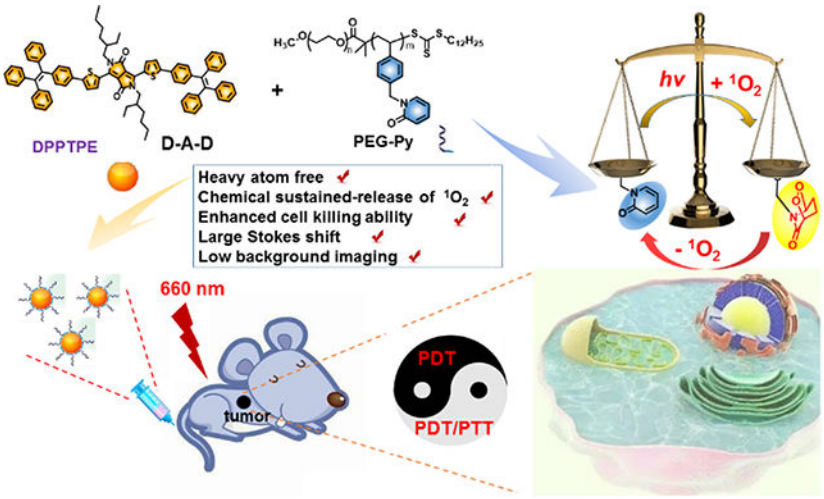

Continuous Photodynamic therapy: The “marriage” of a heavy atom free DPPTPE (Φ_Δ = 69%) and PEG-Py with 2-pyridone for reversibly capturing and releasing $^1O_2$ can improve the lifetime of $^1O_2$ under both normoxic and hypoxic conditions, thus improve the phototherapy efficacy of DPPTPE@PEG-Py NPs, compared with that of DPPTPE@DSPE-PEG NPs as control.

Keywords

heavy atom free; DPPTPE; continuous PDT; theranostics

Photodynamic therapy (PDT) is a promising strategy which can transform nontoxic oxygen to toxic reactive oxygen species (ROS) for cancer treatment. As a result, great efforts have been devoted to advance PDT owing to its unique features, including the lack of initiating resistance, low systemic toxicity, and minimal invasiveness.[1–5] To date, a majority of existing PDT systems depend highly on O_2 concentration and involves a huge consumption of O_2. [6–10] Unfortunately, due to insufficient O_2 in blood supply in the tumor region and aggressive proliferation of cancer cells, O_2 concentration, however, varies from different locations in solid tumors, with some interior regions being extremely low. Thus, O_2 shortage in tumors is responsible for significantly reduced antitumor efficacy of PDT, especially in those cases that require continuous treatment. Therefore, the hypoxia of tumor microenvironment (TME) is universally considered as the “Achilles’ heel” of PDT. [11,12]

To reverse the deficiency of oxygen in TME for sustainable PDT, considerable efforts were made to find efficient and safe strategies to refuel O_2 in TME to boost the PDT efficacy, such as delivering oxygen saturated perfluorocarbons to TME, fabricating inorganic nanoenzymes (such as MnO_2 nanoparticles and nanosheets) to generate oxygen in the acidic TME. However, some concerned issues hinder their practical applications in the clinic. For example, for the fluorocarbons system, the inevitable oxygen leakage from fluorocarbons during the longtime blood circulation usually induces inefficient oxygen delivery. Although the nanoenzymes could produce oxygen effectively in the tumor region, the superfluous metal ion release may bring about acute toxicity, oxidative stress and oxidative damage to main organs. By looking back on the application of PDT in the clinic, fractionated PDT

provides time for the replenishment of cellular oxygen and minimize photoinduced hypoxia.[13–15] In continuous PDT, the chemically collecting and then sustained releasing of partial singlet oxygen from photosensitized generation may enhance the cell killing effect in the PDT induced temporary hypoxia and boost the phototheranostics.

In recent years, semiconducting materials have been widely used for biomedical applications, including imaging and therapy.[16–20] For example, Li *et al.* designed an organic semiconducting pro-nanostimulant for NIR photoactivatable cancer immunotherapy.[16] In addition, a semiconducting polymer based pro-nanoenzyme was fabricated to improve therapeutic specificity.[17] 2-Pyridone group is able to react with singlet oxygen to form endoperoxides of 2-pyridone. The resulting product can undergo thermal cycloreversion to release singlet oxygen *in vivo*, re-producing 2-pyridone module. Thus, the strategy of using 2-pyridone based polymer to encapsulate photosensitizer (PS) could be an attractive approach to fabricating desirable enhanced PDT regents (scheme 1). In this study, we developed an intelligent phototheranostics with the capability of enhanced PDT. The phototheranostics (DPPTPE@PEG-Py NPs) was obtained by nanoprecipitation of a 2-pyridone based amphiphilic diblock polymer (PEG-Py) and a newly synthesized semiconducting pyrrolopyrrolidone-tetraphenylethylene (denoted as DPPTPE) with a high $^1O_2$ quantum yield of 69%. PEG-Py contains abundant 2-pyridone pendants for capturing and then releasing singlet oxygen in the dark cycle. Since DPPTPE is a heavy atom free PS, it would have negligible dark toxicity *in vivo*. As a result, the photodynamic process of DPPTPE@PEG-Py NPs keeps producing $^1O_2$ under the laser irradiation even when O_2 supply is stopped. The chemical storage of $^1O_2$ was also demonstrated in the light as well as dark cycles. The DPPTPE@PEG-Py NPs also showed photothermal effect, providing synergistic photothermal/photodynamic therapy. The enhanced phototheranostic effect was demonstrated by four different cancer cell lines (HeLa, HCT-116, A549 and MCF-7). Furthermore, thanks to the large Stokes shift of DPPTPE, *in vivo* fluorescence imaging with low background guided the phototherapy experiment, in which the tumors treated with DPPTPE@PEG-Py NPs were completely inhibited without any adverse effects to main organs, such as heart, kidneys, liver, lung and spleen. This study demonstrates that DPPTPE@PEG-Py NPs can be a powerful candidate for enhanced phototherapy and also provides a paradigm to develop highly efficient PSs.

General synthetic routes of DPPTPE and PEG-Py are shown in supporting information (figure S1, S2). DPPTPE was prepared through a C-H activation reaction by reacting DPP and Br-substituted tetraphenylethylene in the presence of anhydrous K_2CO_3 and PivOH with $Pd(OAc)_2$ as the catalyst in anhydrous DMA solution.[26] The reversible addition fragmentation chain transfer (RAFT) polymerization method was used for the synthesis of the chlorinated groups based copolymers. Then 2-pyridone was conjugated onto the polymer with the catalysis of hexaoxacyclooctadecane and K_2CO_3 in DMF to form PEG-Py. The structure of DPPTPE was characterized by ^{1}HNMR, ^{13}CNMR and mass spectroscopy (figure S3–S7).

DPPTPE in THF exhibited maximum absorbance at 576 and 618 nm while a red shift was observed after the PEG-Py coated DPPTPE was dispersed in water (589 and 640 nm). Simultaneously, DPPTPE@PEG-Py NPs showed a large Stokes shift (163 nm) and strong

NIR fluorescence, which is helpful for *in vivo* NIR fluorescence imaging (figure 1a). Transmission electron microscope (TEM) and dynamic light scattering (DLS) indicated that size distribution of DPPTPE@PEG-Py NPs was from 52 to 128 nm (figure 1b), which is similar to that of DPPTPE@DSPE-PEG NPs (figure S8). High $^1O_2$ generation is the indispensable property for a PS to achieve effective PDT. The $^1O_2$ quantum yield (QY) of DPPTPE in dichloromethane (DCM) was quantified by using the commercial PDT agent methylene blue (MB) as a standard substance (Φ_Δ = 57% in DCM). The $^1O_2$ QY of DPPTPE was calculated to be as high as 69% (figure 1c, S9 and S10). To investigate the singlet oxygen generation ability of DPPTPE@PEG-Py NPs, singlet oxygen sensor green (SOSG) was used in the experiments (figure 1d, S11). With laser irradiation, the fluorescence intensity of SOSG in the presence of DPPTPE@PEG-Py NPs increased rapidly while that of SOSG alone was negligible.

Then, we demonstrated the continuous PDT property of DPPTPE@PEG-Py NPs by investigating the reversible singlet oxygen capture and release process under different conditions, including normoxia and hypoxia. For the DPPTPE@DSPE-PEG group under normoxic condition, the fluorescence intensity of SOSG increased by 3-fold after 1 min irradiation, indicating effective $^1O_2$ generation. While in the dark, negligible fluorescence enhancement was observed (figure S12). In contrast, the fluorescence intensity of SOSG after irradiation of DPPTPE@PEG-Py for 1 min continued to increase over time in the dark even without irradiation (figure 2a and 2b). This can be explained by the fact that singlet oxygen can be captured by the 2-pyridone to form an endoperoxide during light irradiation and is then chemically released without irradiation (scheme 1). PEG-Py with abundant benzene groups is able to reduce the **π-π** stacking of DPPTPE more efficiently than DSPE-PEG, thereby reducing the ACQ. The amount of generated $^1O_2$ of DPPTPE@PEG-Py NPs is more than that of DPPTPE@DSPE-PEG NPs. Negligible fluorescence enhancement was observed after 45 min, indicating the complete release of $^1O_2$ (half-life of $^1O_2$ release was approximately 1.8 min). In addition, we studied whether the DPPTPE@PEG-Py NPs can still generate $^1O_2$ under hypoxic condition. Thus, the experiment was conducted by irradiating such solution for 1 min. Then the solution was purged with N_2 for 45 min. Compared with DPPTPE@DSPE-PEG, DPPTPE@PEG-Py NPs still showed $^1O_2$ generation when the oxygen was insufficient (figure 2c and 2d), indicating that the DPPTPE@PEG-Py NPs could release $^1O_2$ under hypoxic condition, as well (half-life of $^1O_2$ release was 1.6 min).

Combining PDT with photothermal therapy (PTT) is considered to be a superior way to achieve better phototherapeutic efficacy. Photothermal conversion efficiency was investigated by heating and cooling DPPTPE@PEG-Py NPs (figure S13a, 13b). A temperature elevation of 17.6 ^oC can be observed with laser irradiation, promising the potential for mild photothermal therapy of DPPTPE@PEG-Py NPs. The photothermal conversion efficiency of such NPs is calculated to be 30.6%. A concentration dependent temperature elevation can be observed (figure S13c). The repeated photothermal conversion experiments were performed to investigate the thermal stability (figure S13d). It is worth pointing out that such NPs exhibit excellent photothermal stability after being repeated for at least 5 cycles and no decay was observed in the absorbance spectra (figure S14).

High singlet oxygen generation ability and photothermal conversion efficiency contribute to the high cytotoxicity of PS.[27] To further confirm the phototherapy efficacy of DPPTPE, four different cell lines, HeLa, HCT-116, A549 and MCF-7 were tested. The cellular uptake of NPs was performed by CLSM. Enhanced ROS generation with DCF as a probe can be detected for DPPTPE@PEG-Py NPs due to the enhanced fluorescence intensity, compared with that of DPPTPE@DSPE-PEG (figure 3a, 3b). Furthermore, MTT assay indicated neither DPPTPE@DSPE-PEG nor DPPTPE@PEG-Py NPs was toxic as the cell viabilities of the four groups were similar to those of the control groups without light irradiation (figure S15). In contrast, considerably high phototoxicity of DPPTPE@PEG-Py NPs can be detected on the four different cell lines with laser irradiation (figure 3c–3f), which is superior to those treated with DPPTPE@DSPE-PEG (figure 3c–3f). These results suggest that heavy atom free DPPTPE with high singlet oxygen generation ability are capable of inhibiting cell proliferation. Meanwhile, DPPTPE@PEG-Py NPs with singlet oxygen capture and release ability are superior to DPPTPE@DSPE-PEG, indicating that DPPTPE@PEG-Py NPs are more suitable for cancer treatment.

Furthermore, UV-Vis spectrometry was applied to study the pharmacokinetics after intravenous administration of NPs.[27] The mean plasma concentration-time profiles of DPPTPE@PEG-Py NPs and DPPTPE@DSPE-PEG NPs (figure 4a) were used to calculate the main pharmacokinetic parameters by a non-compartmental model (Table 1). The values of the $AUC_{(0\text{-}t)}/AUC_{(0-\infty)}$ over 80% suggested that the blood collection time point was suitable for the pharmacokinetic study. The data showed that the DPPTPE@DSPE-PEG was eliminated much more quickly than DPPTPE@PEG-Py NPs, with terminal elimination half-lives ($T_{1/2}$) being 4.31 h for DPPTPE@DSPE-PEG and 12.13 h for DPPTPE@PEG-Py, respectively. The CLz of DPPTPE@DSPE-PEG NPs was 0.043 L/h/kg while the value of DPPTPE@PEG-Py NPs was 0.018 L/h/kg, showing that the DPPTPE@PEG-Py NPs were eliminated more slowly than DPPTPE@DSPE-PEG NPs. These results demonstrate that the PEG-Py could extend the residence time and promote its treatment effects.

Fluorescence imaging was used to monitor DPPTPE@PEG-Py NPs accumulation in HeLa tumor for phototheranostics (Figure 4b). The fluorescence intensity of tumor increased after injection of DPPTPE@PEG-Py NPs and reached the peak at 6 h post-injection (figure S16). After imaging study, the mice were sacrificed, followed by the measurement of the intensity of tumor, heart, liver, spleen, lung and kidneys. It was found that these NPs still accumulated in the tumor even at 24 h after injection and the fluorescence intensity of the tumor remained to be the strongest, followed by liver and kidneys (figure S17).

To further investigate the PDT and PTT synergistic therapeutic efficacy of DPPTPE@PEG-Py NPs *in vivo*, 20 nude mice bearing HeLa tumors were divided into four groups as PBS + laser, DPPTPE@DSPE-PEG, DPPTPE@PEG-Py NPs and DPPTPE@PEG-Py NPs + laser groups. To characterize the photothermal ability of DPPTPE@PEG-Py NPs *in vivo*, the tumors were irradiated with laser and the thermal images were captured by an IR camera at 6 h post-injection of DPPTPE@PEG-Py NPs or DPPTPE@DSPE-PEG (figure S18a). The temperature of the group treated with DPPTPE@PEG-Py NPs only increased slightly compared to that of DPPTPE@DSPE-PEG (figure S18b). Then the mice were observed for 18 days and the survival was shown in figure S19. The tumor volume of the group treated

with DPPTPE@PEG-Py NPs is similar to that of the control group, indicating the negligible dark toxicity of DPPTPE@PEG-Py NPs (figure 4c). In contrast, the tumor volume, however, has been significantly suppressed for the illumination groups. And the tumor volume of the group incubated with DPPTPE@PEG-Py NPs is much smaller than that of DPPTPE@DSPE-PEG, suggesting the high phototoxicity of the NPs. It is worth noting that the tumors even disappeared after treatment with DPPTPE@PEG-Py NPs plus laser, indicating that continuous delivery of $^1O_2$ show better phototherapy efficacy. Afterwards, all the mice were further observed for another 10 days, no recurrence of the tumor was observed. The mouse body weight was recorded every two days and no significant change in three groups was observed, demonstrating the biosafety of NPs treatment (figure 4d). The hematoxylin and eosin (H&E)- staining showed that the tumor cells subjected to the DPPTPE@PEG-Py NPs suffered from the largest extent of apoptosis and necrosis (figure 4e–g). After the treatment, all the mice were sacrificed and the tumors were collected as well as the normal organs, including heart, spleen, liver, lung and kidneys. According to the H&E staining images, no abnormal cell morphology can be found between control and DPPTPE@PEG-Py NPs or DPPTPE@DSPE-PEG NPs treated groups in the normal organs (figure S20). In addition, the blood index, renal function and liver function of the mice injected with DPPTPE@PEG-Py NPs or DPPTPE@ DSPE-PEG NPs were the same as those in the control group (Table S1). The results indicated that DPPTPE@PEG-Py NPs could inhibit tumor growth effectively without side effects towards normal organs, suggesting their good biocompatibility[28–39].

In summary, a semiconducting heavy atom free DPPTPE compound with high singlet oxygen generation ability and large Stokes shift of 163 nm has been designed and prepared. 2-pyridione functionalized PEG-Py has been fabricated to encapsulate DPPTPE for reversible capture and release of $^1O_2$ for continuous PDT. In the light cycle, the endoperoxide of 2-pyridone can be generated accompanied by singlet oxygen. In the dark cycle, the endoperoxide undergoes thermal cycloreversion to deliver singlet oxygen, regenerating the 2-pyridone module. The as-prepared DPPTPE@PEG-Py NPs work under both normoxic and hypoxic conditions and are more efficacious in tumor killing than that of DPPTPE@DSPE-PEG NPs. Furthermore, *in vivo* fluorescence imaging guided phototherapy suggests DPPTPE@PEG-Py NPs with high phototoxicity as well as low dark toxicity are potential candidates for phototheranostics.

Supplementary Material

Refer to Web version on PubMed Central for supplementary material.

Acknowledgements

The work was supported by the NNSF of China (61525402, 61775095, 21704043, 81872255), Jiangsu Provincial key research and development plan (BE2017741), Six talent peak innovation team in Jiangsu Province (TD-SWYY-009, WSW041), the NSF of Jiangsu Province (BK20170990, 17KJB150020), Key medical talents fund of Jiangsu Province (2016KJQWZDRC-03) and the China Scholarship Council and intramural research program of the National Institute of Biomedical Imaging and Bioengineering (NIBIB), National Institutes of Health (NIH).

References

[1]. Castano AP, Mroz P, Hamblin MR, Nat. Rev. Cancer 2006, 6, 535–545. [PubMed: 16794636]

[2]. Celli JP, Spring BQ, Rizvi I, Evans CL, Samkoe KS, Verma S, Pogue BW, Hasan T, Chem. Rev 2010, 110, 2795–2838. [PubMed: 20353192]

[3]. Li X, Lee S, Yoon J, Chem. Soc. Rev 2018, 47, 1174–1188 [PubMed: 29334090]

[4]. Zou JH, Wang P, Wang Y, Liu GY, Zhang YW, Zhang Q, Shao JJ, Si WL, Huang W, Dong XC, Chem. Sci, 2019, 10, 268–276. [PubMed: 30713637]

[5]. Ye SY, Rao JM, Qiu SH, Zhao JL, He H, Yan ZL, Yang T, Deng YB, Ke HT, Yang H, Zhao YL, Guo ZQ, Chen HB, Adv. Mater, 2018, 30, 1801216.

[6]. Brown JM, Wilson WR, Nat. Rev. Cancer, 2004, 4, 437–447. [PubMed: 15170446]

[7]. Shen J, Chen JJ, Ke Z, Zou DF, Sun LG, Zou JH, Mater. Chem. Front,2019, 3, 1123–1127.

[8]. Tsai YC, Vijayaraghavan P, Chiang WH, Chen HH, Liu TI, Shen MY, Omoto A, bKamimura M, Sog K, Chiu HC, Theranostics 2018, 8, 1435–1447. [PubMed: 29507632]

[9]. Zou JH, Yin ZH, Wang P, Chen DP, Shao JJ, Zhang Q, Sun LG, Huang W, Dong XC, Chem. Sci 2018, 9, 2188–2194. [PubMed: 29719692]

[10]. Li RQ, Zhang C, Xie BR, Yu WY, Qiu WX, Cheng H, Zhang XZ, Biomaterials, 2019, 194, 84–93 [PubMed: 30583151]

[11]. Yang Z, Chen XY, Acc. Chem. Res 2019, 52, 1245–1254. [PubMed: 30977625]

[12]. Fan WP, Huang P, Chen XY, Chem. Soc. Rev, 2016, 45, 6488–6519. [PubMed: 27722560]

[13]. Turan IS, Yildiz D, Turksoy A, Gunaydin G, Akkaya EU, Angew. Chem. Int. Ed, 2016, 55, 2875–2878.

[14]. Xiao WY, Wang P, Ou CJ, Huang XY, Tang YY, Wu MY, Si WL, Shao JJ, Huang W, Dong XC, Biomaterials, 2018, 183, 1–9. [PubMed: 30142531]

[15]. Turan IS, Yildiz D, Turksoy A, Gunaydin G, Akkaya EU, Angew.Chem. Int. Ed 2016, 55, 2875–2878.

[16]. Li JC, Cui D, Huang JG, He SS, Yang ZB, Zhang Y, Luo Y, Pu KY, Angew. Chem. Int. Ed 2019, 58, 12680–1268

[17]. Li JC, Huang JG, yu Yan L., Huang JS, Jiang YY, Xie C, Pu KY, J. Am. Chem. Soc2019, 141, 4073–4079 [PubMed: 30741538]

[18]. Zhu HJ, Li JC, Qi XY, Chen P, Pu KY. Nano Lett. 2018, 18, 58–594 [PubMed: 29190106]

[19]. Cui D, Huang JG, Zhen X, Li JC, Jiang YY, Pu KY, Angew. Chem. Int. Ed 2019, 58, 5920–5924

[20]. Lyu Y, Zeng JF, Jiang YY, Zhen X, Wang T, Qiu SS, Lou X, Gao MY, Pu KY, ACS Nano, 2018, 12, 1801–1810 [PubMed: 29385336]

[21]. Zhu HJ, Fang Y, Zhen X, Wei N, Gao Y, Luo KQ, Xu CJ, Duan HW, Ding D, Chen P, Pu KY, Chem. Sci,2016,7,5118–5125 [PubMed: 30155162]

[22]. Xiao Z, Halls S, Dickey D, Tulip J, Moore RB, Clin. Cancer Res 2007, 13, 7496–7505 [PubMed: 18094434]

[23]. Yang L, Chen Q, Wei Y, Xing D, Lasers Surg. Med 2010, 42, 671–679. [PubMed: 20740620]

[24]. Bisland SK, Lilge L, Lin A, Rusnow R, Wilson BC, Photochem. Photobiol 2004, 80, 22–30. [PubMed: 15339204]

[25]. de Souza AL, Marra K, Samkoe KS, Kanick SC, Davis SC, Chapman MS, Maytin EV, Hassan T, Pogue BW, Br. J. Cancer 2016, 115, 805–813. [PubMed: 27575852]

[26]. Liu SY, Shi MM, Huang JC, Jin ZN, Hu XL, Pan JY, Li HY, Jen Alex K.Y., Chen HZ, J. Mater. Chem. A, 2013, 1, 2795–2805.

[27]. Zou JH, Yin ZH, Ding KK, Tang QY, Li JW, Si WL, Shao JJ, Zhang Q, Huang W, Dong XC, ACS Appl Mater Interfaces., 2017, 9, 32475–32481. [PubMed: 28875695]

[28]. Zhu JW, Zou JH, Zhang ZJ, Zhang J, Sun Y, Dong XC, Zhang Q, Mater. Chem. Front, 2019, 3, 1523–1531

[29]. Shen J, Chen JK, Ke Z, Zou DF, Sun LG, Zou JH, Mater. Chem. Front, 2019, 3, 1123–1127.

[30] (a). Yang Z, Tian R, Wu J, Fan QL, Yung BC, Niu G, Jacobson O, Wang ZT, Liu G, Yu G, Huang W, Song JB, Chen XY, ACS Nano, 2017, 11, 4247–4255. [PubMed: 28345873] (b)Zhang L,

Yang XQ, Wei JS, Li X, Wang H, Zhao YD, Theranostics, 2019, 9, 5424–5442. [PubMed: 31534494]

[31]. Yang Z, Dai YL, Yin C, Fan QL, Zhang W, Song JB, Yu GC, Tang W, Fan WP, Yung BC, Li J, Li X, Li X, Tang Y, Huang W, Song JB, Chen XY, Adv. Mater, 2018, 30, 1707509.

[32]. Yang J, Gu XQ, Su WT, Hao XY, Shi YJ, Zhao LY, Zou DF, Yang GW, Li QY, Zou JH, Mater. Chem. Front, 2018, 2, 1842–1846.

[33]. Yang Z, Song JB, Tang W, Fan WP, Dai YL, Shen ZY, Lin LS, Cheng S, Liu Y, Niu G, Rong P, Wang W, Chen XY, Theranostics, 2019, 9, 526. [PubMed: 30809290]

[34]. Yang Z, Song J, Dai Y, Chen J, Wang F, Lin L, Liu Y, Zhang F, Yu G, Zhou Z, Fan W, Huang W, Fan Q and Chen XY, Theranostics, 2017, 7, 2177. [PubMed: 28740543]

[35]. Huang L, Li ZJ, Zhao Y, Yang JY, Yang YC, Pendharkar AI, Zhang YW, Kelmar S, Chen LY, Wu WT, Zhao JZ, Han G, Adv. Mater 2017, 29, 1604789.

[36]. Zhu T, Shi LL, Yu CY, Dong YB, Qiu F, Shen LY, Qian QH, Zhou GY, Zhu XY, Theranostics, 2019, 9, 3293–3307. [PubMed: 31244955]

[37]. Gu BB, Wu WB, Xu GX, Feng GX, Yin F, Joo Chong PH, Qu JL, Yong KT, Liu B, Adv. Mater 2017, 1701076.

[38]. Huang ZQ, Wei GF, Zeng ZS, Huang YJ, Huang LF, Shen YF, Sun XQ, Xu CJ, Zhao CS, Theranostics, 2019, 9, 5542–5557. [PubMed: 31534502]

[39]. Zhuang WH, Ma BX, Hu J, Jiang JZ, Li GC, Yang L, Wang YB, Theranostics, 2019, 9, 6618–6630. [PubMed: 31588239]

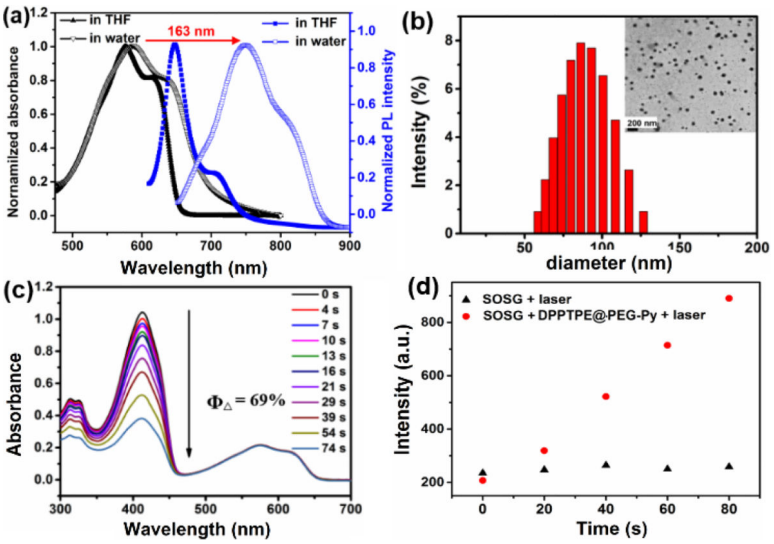

Figure 1.

(a) Normalized absorbance and fluorescence spectra of DPPTPE in THF and NPs in water; (b) TEM and DLS of DPPTPE@PEG-Py NPs; (c) Singlet oxygen generation of DPPTPE in DCM with DPBF as a probe; (d) Singlet oxygen generation of DPPTPE@PEG-Py NPs with SOSG as a probe.

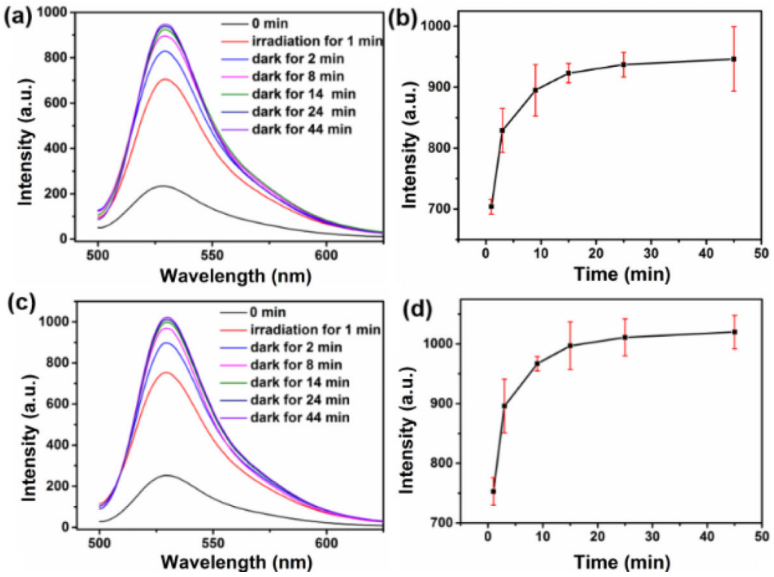

Figure 2.

Singlet oxygen capture and release of DPPTPE@PEG-Py NPs with irradiation for 1 min and then in dark for 44 min: (a-b) under normoxia condition; (c-d) under hypoxia condition with N_2 bubbling after 1 min irradiation.

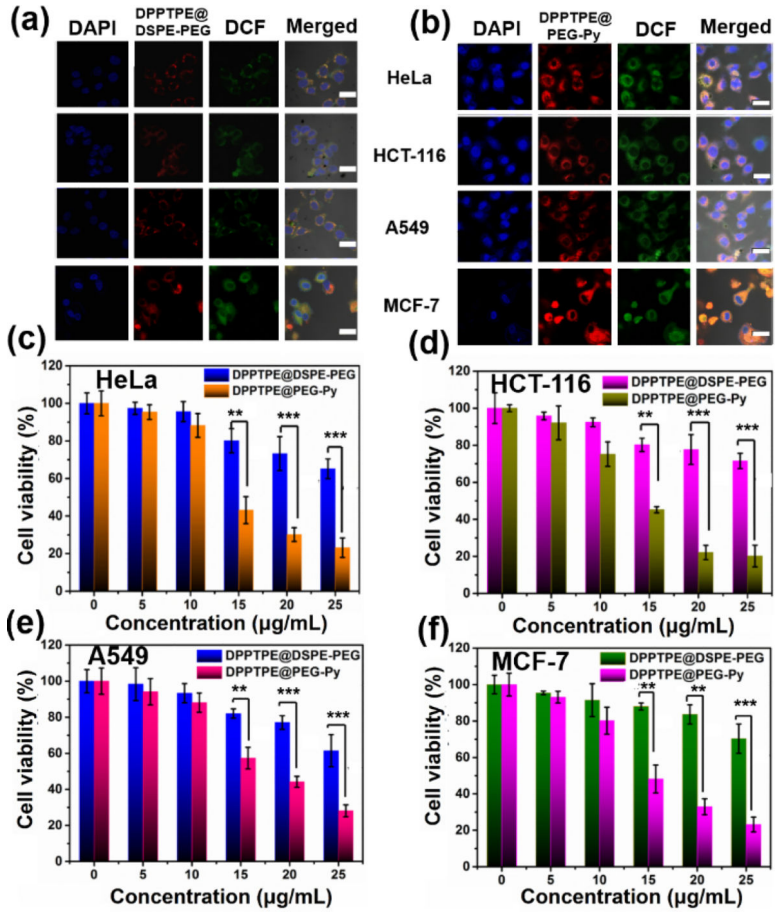

Figure 3.

Cellular uptake of (a) DPPTPE@DSPE-PEG; (b) DPPTPE@PEG-Py NPs in HeLa, HCT-116, A549 and MCF-7 cells, scale bar: 10 μm; MTT assay of (c) HeLa; (d) HCT-116; (e) A549 and (f) MCF-7 with treatment of DPPTPE@DSPE-PEG and DPPTPE@PEG-Py NPs with laser irradiation (660 nm, 0.1 W/cm^2). (**p<0.01 and ***p<0.001 compared with the control group)

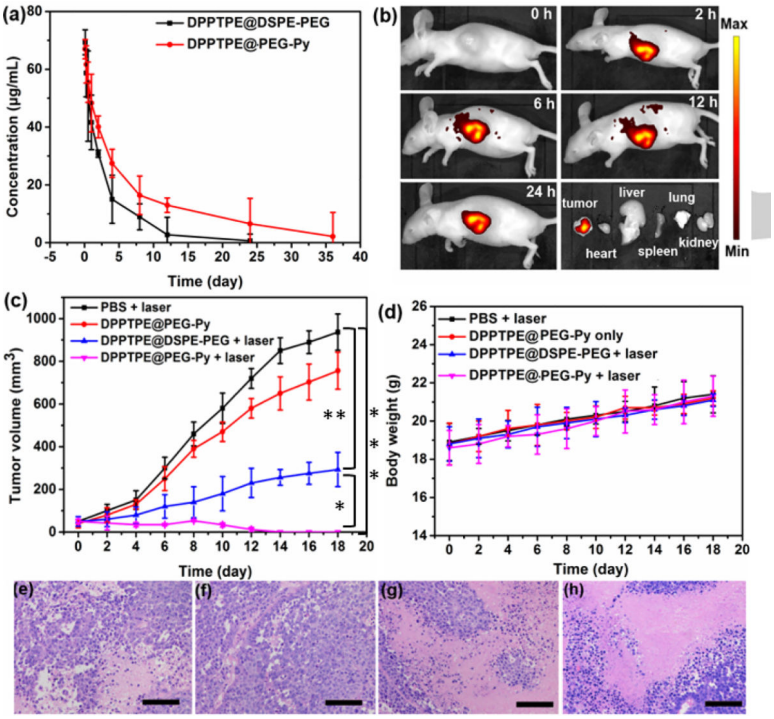

Figure 4.

(a) Mean plasma time dependent drug concentration curves of DPPTPE@PEG-Py NPs or DPPTPE@DSPE-PEG NPs after a single intravenous administration at a dose of 5 mg/kg in rat; (b) *In vivo* fluorescence imaging of HeLa tumor bearing mouse for different period of time; (c) Tumor volume change (*$p < 0.05$, **$p < 0.01$ and ***$p < 0.001$ compared with the control group); (d) Body weight change during the treatment. H&E stained pictures of the tumor cells. (e) PBS + laser; (f) DPPTPE@PEG-Py NPs; (g) DPPTPE@DSPE-PEG + laser. Scale bar: 100 μm.

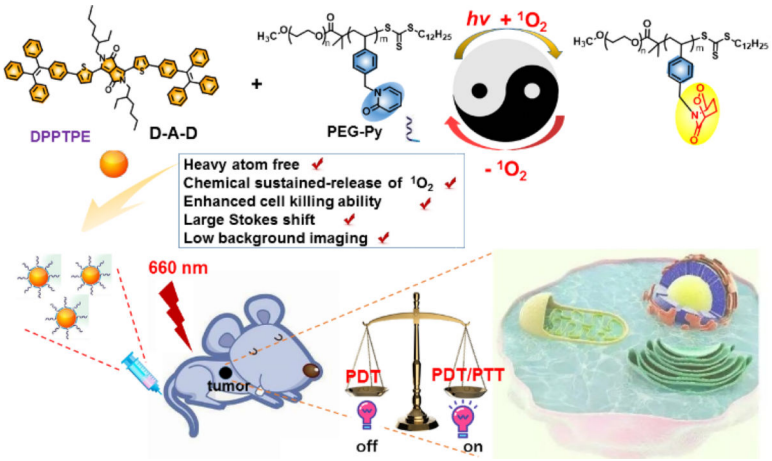

Scheme 1.

Schematic of light responsive PEG-Py with $^1O_2$ capture and release ability for phototheranostics.

Table 1

Non-compartmental pharmacokinetic parameters of DPPTPE@DSPE-PEG or DPPTPE@PEG-Py NPs in rat plasma after a single intravenous administration at a dose of 5 mg/kg (n=6/group)

Parameter	DPPTPE@DSPE-PEG	DPPTPE@PEG-Py
$T_{1/2}$	4.31	12.13
$AUC_{(0-t)}$	226.9	484.4
$AUC_{(0-\infty)}$	230.9	542.2
$MRT_{(0-t)}$	4.22	9.55
VZ	0.27	0.32
CL_Z	0.043	0.018

$T_{1/2}$: terminal elimination half-life; $AUC_{(0-t)}$: the area under the curve from zero to the last measurable plasma concentration point; $AUC_{(0-\infty)}$: the area under the curve from zero to infinity; $MRT_{(0-t)}$: mean residence time; V_Z: apparent volume of distribution; CLz: systemic clearance.